REGULAR ARTICLE

blood advances

Clearing and replacing tissue-resident myeloid cells with an anti-CD45 antibody–drug conjugate

Karin Gustafsson,[1-3] Catherine Rhee,[1-3] Vanessa Frodermann,[4] Elizabeth W. Scadden,[1-3] Dan Li,[1-3] Yoshiko Iwamoto,[4] Rahul Palchaudhuri,[5] Sharon L. Hyzy,[5] Anthony E. Boitano,[5] Matthias Nahrendorf,[4] and David T. Scadden[1-3]

[1]Center for Regenerative Medicine, Massachusetts General Hospital, Boston, MA; [2]Harvard Stem Cell Institute, Cambridge, MA; [3]Department of Stem Cell and Regenerative Biology, Harvard University, Cambridge, MA; [4]Center for Systems Biology and Department of Radiology, Massachusetts General Hospital and Harvard Medical School, Boston, MA; and [5]Magenta Therapeutics, Cambridge, MA

Key Points

- Antibody–drug conjugates can deplete tissue-resident macrophages.
- Antibody–drug conjugate conditioning and adoptive cell transfer can alter the disease course of inflammatory conditions.

Tissue-resident myeloid (TRM) cells in adults have highly variable lifespans, and may be derived from early embryonic yolk sac, fetal liver, or bone marrow. Some of these TRM cells are known pathogenic participants in congenital and acquired diseases. Myeloablative conditioning and hematopoietic stem cell transplantation can replace long-lived brain TRM cells, resulting in clinical improvements in metabolic storage diseases. With the advent of antibody–drug conjugate (ADC)-targeted cell killing as a cell-selective means of transplant conditioning, we assessed the impact of anti-CD45–ADC on TRM cells in multiple tissues. Replacement of TRM cells ranged from 40% to 95% efficiencies in liver, lung, and skin tissues, after a single anti-CD45–ADC dose and bone marrow hematopoietic cell transfer. Of note, the population size of TRM cells in tissues returned to pretreatment levels, suggesting a regulated control of TRM cell abundance. As expected, brain microglia were not affected, but brain monocytes and macrophages were 50% replaced. Anti-CD45–ADC and adoptive cell transfer were then tested in the chronic acquired condition, atherosclerosis exacerbated by *Tet2* mutant clonal hematopoiesis. Plaque-resident myeloid cells were efficiently replaced with anti-CD45–ADC and wild-type bone marrow cells. Notably, this reduced existent atherosclerotic plaque burden. Overall, these results indicate that the anti-CD45–ADC clears both hematopoietic stem and TRM cells from their niches, enabling cell replacement to achieve disease modification in a resident myeloid cell–driven disease.

Introduction

Antibody–drug conjugates (ADCs) may be an efficient way of depleting endogenous hematopoiesis to make way for an incoming cell graft while circumventing many of the liabilities of broad cytotoxic interventions like irradiation or chemotherapy. ADC-mediated conditioning allows for selective delivery of a toxic payload, limiting off-target effects, and has been shown to minimize the duration of immunodeficiency.[1-4] However, because of the biodistribution properties of antibodies, questions have been raised as to its potential application to conditions in which mature leukocytes and not just bone marrow–residing hematopoietic stem and progenitors (HSPCs) need to be replaced.[5]

Submitted 31 May 2023; accepted 8 September 2023; prepublished online on *Blood Advances* First Edition 25 September 2023; final version published online 17 November 2023. https://doi.org/10.1182/bloodadvances.2023010561.

Original data are available on request from the corresponding author, David T. Scadden (david_scadden@harvard.edu).

The full-text version of this article contains a data supplement.

Many tissues contain myeloid cell populations that are bone marrow independent, so-called tissue-resident myeloid (TRM) cells. Brain microglia are descendants of the first wave of hematopoietic progenitors that originate in the yolk sac.[6,7] In other organs such as the liver, lung and skin TRM cells are primarily derived from later fetal hematopoietic waves.[8,9] These tissue-specific myeloid cells will mostly remain bone marrow independent throughout life unless tissue homeostasis is disrupted.[10] Liver Kupffer cells, for instance, can be depleted by inflammatory injury, leading to the subsequent recruitment of bone marrow–derived monocytes that will eventually differentiate into Kupffer cells.[11,12] Likewise, although initially monocyte derived, the majority of macrophages in advanced atherosclerotic plaques self-renew to maintain their numbers rather than relying on continuous import of cells from the bone marrow.[13] Conventional hematopoietic stem cell transplantation (HSCT) conditioning regimens replace TRM cells efficiently in most tissues, including the central nervous system.[10,14-18] Antibodies, however, will penetrate solid tissues to varying degrees because of their large size and polarity. The sinusoidal vessel network of the bone marrow leads to efficient antibody uptake, but other tissue types with more restrictive vascular beds such as the skin or brain will see a more limited distribution. An ADC that facilitates excellent bone marrow conditioning and HSPC engraftment could thus still fail to replace some TRM cell populations.

We set out to test whether a newly developed ADC targeting the leukocyte-restricted, pan-hematopoietic marker CD45 would be able to also deplete tissue-resident populations of myeloid cells, leading to their replacement upon bone marrow cell transfer. We demonstrate that CD45-ADC and bone marrow cell infusion can lead to complete or near complete substitution of myeloid cells in the skin, lung, and liver. Furthermore, in a model of clonal hematopoiesis and atherosclerosis, CD45-ADC treatment followed by bone marrow cell transplantation leads to highly efficient depletion of disease-driving leukocytes in both bone marrow and atherosclerotic plaques, leading to disease mitigation.

Methods

ADC

The CD45-ADC and its cognate isotype control–ADC have been reported previously (Magenta Therapeutics).[4] In brief, CD45.2 clone 104 was engineered for increased in vivo clearance and conjugated to the pyrrolobenzodiazepine cytotoxic payload.

Animals

ADC conditioning and HSCT experiments in wild-type (WT) mice were carried out in 8-week-old male and female C57BL/6J mice. For modeling of atherosclerotic disease, 8-week-old make and female B6.129S7-Ldlrtm1Her/J low density lipoprotein receptor (*Ldlr*) gene–knockout (KO) female and male mice were used. Donors of green fluorescent protein (GFP)-labeled WT marrow were C57BL/6-Tg(UBC-GFP)30Scha/J mice, and B6.SJL-Ptprca Pepcb/BoyJ mice were used as CD45.1 donors. *Tet2* KO mouse strain B6;129S-Tet2tm1.1Iaai/J was crossed to B6.Cg-Tg(Mx1-cre)1Cgn/J and B6.129(ICR)-Tg(CAG-ECFP)CK6Nagy/J to generate cyan fluorescent protein (CFP)-labeled conditional *Tet2* WT and KO donors for clonal hematopoiesis modeling. All mice were obtained from Jackson Laboratories and all animal experimentation was carried out in accordance with national and institutional guidelines and with the approval of the institutional animal care and use committee of Massachusetts General Hospital.

ADC conditioning and HSCT

Recipient mice, unless otherwise specified, received retro-orbital injections of isotype-ADC or CD45-ADC (3 mg/kg body weight), and 48 to 72 hours after ADC administration, 2.0×10^7 congenic bone marrow cells from donor mice were injected retro-orbitally. Donor bone marrow was prepared by CO_2 asphyxiation of *ubiquitin-GFP* or CD45.1$^+$ donor mice, followed by dissection of femurs, tibias, pelvis, and vertebral column. Bone marrow cells were isolated by crushing the bones gently in phosphate buffered saline (PBS; ThermoFisher Scientific) supplemented with 2% (v/v) fetal bovine serum (FBS, Gibco) and passing the resultant cell suspension over a 70-μm cell strainer (BD Falcon). Recipient mice were euthanized for tissue isolation, 6 weeks after HSCT.

Modeling clonal hematopoiesis

Ldlr KO recipient mice received a split dose of 12 Gray irradiation from a ^{137}Cs source, 24 hours before graft injection. Donor bone marrow was prepared as described earlier. The graft consisted of either 200 000 *Tet2$^{fl/f}$MxCre-βactin-CFP* and 800 000 *Ubiquitin-GFP* bone marrow cells or 200 000 *Tet2$^{WT/WT}$MxCre-βactin-CFP* and 800 000 *Ubiquitin-GFP* bone marrow cells, and was delivered via retro-orbital injection. Cre-mediated deletion of the floxed *Tet2* allele was induced 4 weeks after transplantation by 4 injections of 12.5 μg/mL polycytidylic acid (Cytiva) every other day.

Atherosclerosis modeling

To induce atherosclerosis, *Ldlr* KO mice were placed on a rodent atherogenic diet (1.25% cholesterol, regular casein; Research Diets Inc) for a total of 12 weeks. In *Tet2*-mutant clonal hematopoiesis experiments, mice were allowed to recover for 4 weeks before being placed on the atherogenic diet.

Blood sampling

Depending on the experiment, mice were bled at 4, 6, 8, 12, and 16 weeks after transplantation, or at 6 weeks after transplantation. All blood collection was performed via retro-orbital puncture under isoflurane anesthesia, and blood was collected into ethylenediaminetetraacetic acid (EDTA)-coated tubes to prevent coagulation. Complete blood counts were obtained using the Element HT5 Auto Hematology system (Heska).

Tissue collection

For all tissue collections, the mice were anesthetized using vaporized isoflurane (3%-4%) and anesthesia depth was assessed by toe pinching. Transcardial perfusion was thereafter performed with 40 mL of PBS (ThermoFisher Scientific). For isolation of the lungs, 5 to 10 mL of PBS (ThermoFisher Scientific) was also flushed through the right ventricle. The liver was slowly perfused with an additional 30 mL of PBS (ThermoFisher Scientific), through the portal vein.

Skin was isolated from mouse ears.[19] In brief, ears were excised 2 mm above their base. The internal and external faces of the ear were then separated gently by forceps and placed, cartilage side down, in PBS (ThermoFisher Scientific) with 50 mM

N-2-hydroxyethylpiperazine-*N*′-2-ethanesulfonic acid (HEPES; Gibco) and 0.4 mg/mL (w/v) dispase II (Gibco). The tissue was incubated for 2 hours at 37°C. Ear cartilage was thereafter scraped off gently, and the remaining skin tissue finely minced and subjected to 2 rounds of digestion in RPMI 1640 (Gibco) with 50 mM HEPES (Gibco), 2 mg/mL (w/v) collagenase IV (Millipore Sigma) and 6 U/mL DNase I (ThermoFisher Scientific) at 37°C and 750 g for 30 minutes. The resulting single-cell suspension was passed through a 100-μm cell strainer (BD Falcon) and thereafter washed with PBS supplemented with 10% (v/v) FBS (Gibco). Finally, ammonium-chloride-potassium (ACK) lysis (Quality Biological) for 5 minutes at room temperature was used for removal of erythroid cells.

Brains were carefully dissected, cut into small pieces, and further mechanically dissociated using a p1000 micropipette.[20] The tissue was then enzymatically dissociated using a Multi-tissue Dissociation Kit I (Miltenyi) for 30 minutes at 37°C and 750 rpm, with intermittent trituration. The cell suspension was filtered over a 100-μm cell strainer (BD Falcon) and thereafter washed with PBS (ThermoFisher Scientific) supplemented with 10% (v/v) FBS (Gibco). The samples were further cleaned-up by Debris Removal solution (Miltenyi), and, finally, red blood cells were lysed using ACK lysis buffer (Quality Biological).

Liver hematopoietic cells were isolated by careful mincing of hepatic tissue followed by enzymatic dissociation in RPMI 1640 with 50 mM HEPES (Gibco), 1 mg/mL collagenase IV, and 6 U/mL DNase I (ThermoFisher Scientific) at 37°C and 750 rpm for 30 minutes.[21,22] The liver cell suspension was then passed through a 100-μm cell strainer (BD Falcon) and thereafter washed with RPMI 1640 supplemented with 10% (v/v) FBS (Gibco). Hepatocytes were removed by centrifuging samples for 3 minutes at 50*g*, followed by careful collection of supernatant only. Residual erythrocytes were removed by a 5-minute incubation with ACK lysis buffer at room temperature (Quality Biological).

Lungs were dissected and minced before being enzymatically digested for 30 minutes at 37°C and 750 rpm with RPMI 1640 supplemented with 50 mM HEPES (Gibco), 400 μg/mL Liberase (Roche), and 6 U/mL DNase I (ThermoFisher Scientific).[23,24] The digested samples were then filtered across a 100-μm cell strainer (BD Falcon) and thereafter washed with RPMI 1640 supplemented with 10% (v/v) FBS (Gibco). Erythrocytes were lysed with ACK lysis buffer (Quality Biological) and a 5-minute incubation at room temperature.

The entire aorta was harvested from the root to the iliac bifurcation.[13] The aortic root was set aside for histology, and the rest of the tissue was cut finely and then incubated in PBS supplemented with 450 U/mL collagenase I (Millipore Sigma), 125 U/mL collagenase XI (Millipore Sigma), 6 U/mL DNase I (ThermoFisher Scientific), and 60 U/mL hyaluronidase (Millipore Sigma) for 1 hour at 37°C while shaking at 750 rpm. The resulting cell suspension was then passed over a 100-μm cell strainer (BD Falcon) and washed with RPMI 1640 (Gibco) supplemented with 10% (v/v) FBS (Gibco).

Bone marrow was isolated from dissected femurs that were gently crushed in PBS with 2% (v/v) FBS and subsequently filtered over a 70-μm cell strainer (BD Falcon). Red-cell lysis was done by incubating samples with ACK lysis buffer (Quality Biological) for 5 minutes at room temperature.

Fluorescence-activated cell sorting (FACS) analysis of blood

Red blood cells were lysed with ACK lysis buffer (Quality Biological) for 5 minutes at room temperature. Samples were centrifuged at 800*g* for 5 minutes and resuspended in PBS (ThermoFisher Scientific) with 2% (v/v) FBS (Gibco). Samples were blocked for 10 minutes with murine Fc block (BD Biosciences) at 4°C. The samples were then stained with the blood lineage antibody panel (supplemental Table 1) for 30 minutes at 4°C, and then washed with PBS (ThermoFisher Scientific) with 2% (v/v) FBS (Gibco). The samples were resuspended in PBS (ThermoFisher Scientific) with 2% (v/v) FBS (Gibco) and 0.25 μg 7-aminoactinomycin D (BD Biosciences) and analyzed on a BD FACS Aria III (BD Biosciences).

FACS analysis of bone marrow

Bone marrow samples were stained with bone marrow HSPC antibody panels I or II (supplemental Table 1) and incubated at 4°C for 60 minutes. Samples were washed and subsequently stained with 1.5 μg/mL streptavidin-BV650 (Biolegend) for 20 minutes at 4°C. The cells were washed and resuspended in PBS (ThermoFisher Scientific) with 2% (v/v) FBS (Gibco) and 0.25 μg 7-aminoactinomycin D (BD Biosciences), and analyzed on a BD FACS Aria III (BD Biosciences).

FACS analysis of tissue-resident macrophages

Brain, skin, lung, and liver single-cell suspensions were incubated with murine Fc block for 10 minutes at 4°C. The cells were subsequently stained with their respective tissue-specific antibody panels (supplemental Table 1) for 45 minutes at 4°C. The samples were washed with PBS (ThermoFisher Scientific) with 2% (v/v) FBS (Gibco). Lung samples were further incubated with 1.5 μg/mL streptavidin-BV785 (Biolegend) and then washed again. After the final wash, all samples were resuspended in PBS (ThermoFisher Scientific) with 2% (v/v) FBS (Gibco) and 1 μg/mL 4′,6-diamidino-2-phenylindole (DAPI), and analyzed on a BD FACS Aria III (BD Biosciences).

FACS analysis of aorta

Single-cell suspensions of aortic tissue were blocked with murine Fc block for 10 minutes at 4°C. The samples were then stained with aorta antibody panel (supplemental Table 1) for 30 minutes at 4°C, followed by a wash in PBS (ThermoFisher Scientific) with 2% (v/v) FBS (Gibco). Before analysis, the samples were resuspended in PBS (ThermoFisher Scientific) with 2% (v/v) FBS (Gibco) and 1 μg/mL DAPI, and analyzed on a BD FACS Aria III (BD Biosciences).

Histology

Aortic roots were dissected and embedded in Tissue-Tek O.C.T. (Sakura Finetek), snap frozen with dry ice–cooled 2-methylbutane (Fisher Scientific), and subsequently sectioned into 6-μm slices. To ensure lesion size was accurately estimated between treatment groups, sections that captured the maximum lesion area were used. Lesion size was visualized by Oil-red-O (Millipore Sigma) staining, and counterstained with Harris hematoxylin (Millipore Sigma). Lesion size was assessed using NanoZoomer 2.0RS (Hamamatsu). Briefly, lesion area was quantified by measuring the

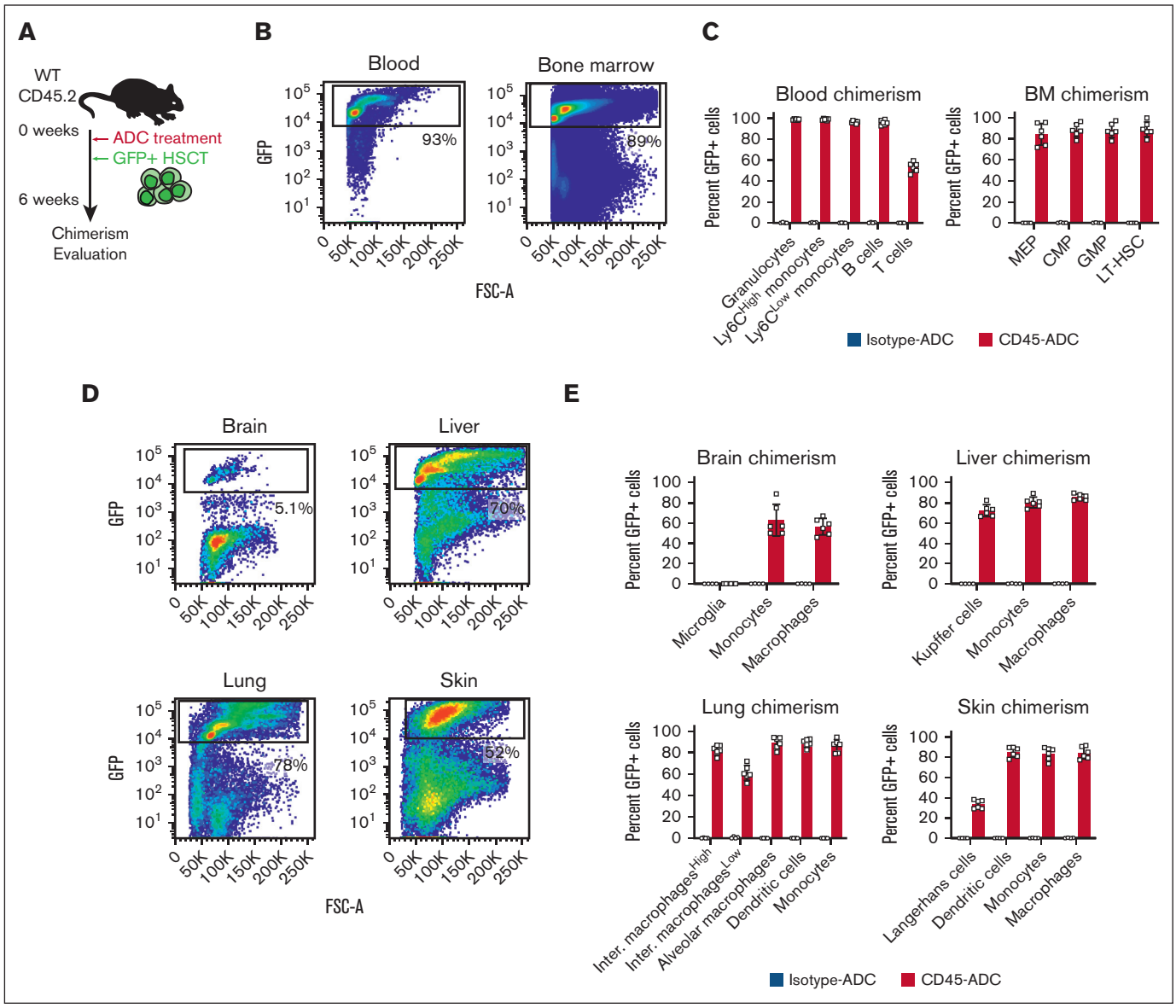

Figure 1. CD45-ADC conditioning enables efficient engraftment in multiple peripheral tissues. (A) Schematic depiction of the experimental design for CD45-ADC treatment and ubiquitin-GFP HSCT. (B) Representative flow plots showing the degree of GFP chimerism in the peripheral blood and bone marrow, 6 weeks after CD45-ADC treatment and HSCT. (C) Bar graphs displaying the flow cytometric analysis of GFP chimerism in peripheral blood and bone marrow cell subsets, 6 weeks after CD45-ADC treatment and HSCT. (D) Flow cytometric analysis plots representative of hematopoietic GFP chimerism in the brain, liver, lung, and skin, 6 weeks after treatment with CD45-ADC and HSCT. (E) The GFP chimerism in various myeloid cell populations in the brain, liver, lung, and skin, as assessed by flow cytometry, 6 weeks after CD45-ADC and HSCT, summarized in bar graphs. CMP, common myeloid progenitor; GMP, granulocyte-monocyte progenitor; Inter. macrophages^{High}, major histocompatibility complex II (MHCII)-high interstitial macrophages; Inter. macrophages^{Low}, MHCII-low interstitial macrophages; MEP, megakaryocyte-erythroid progenitor.

atherosclerotic plaque of the intima from the endothelial layer to the healthy media. For GFP staining, anti-GFP antibody (1:400; ab13970, Abcam) was incubated overnight at 4°C and Alexa Fluor 488 goat anti-chicken immunoglobulin Y (H+L) secondary antibody (1:100; A-11039, ThermoFisher Scientific) was applied to detect GFP$^+$ cells. The tissue sections were counterstained with DAPI (1:3000; D21490, ThermoFisher Scientific), and all the slides were scanned by a digital scanner NanoZoomer 2.0RS.

Statistical analysis

Statistical tests and figures were generated using Prism version 9.1.0. Sample sizes were chosen based on previous experiments and no statistical methods were employed to predetermine sample size. For pairwise comparisons statistical significance was calculated using unpaired, 2-tailed *t* test, and for comparisons between ≥3 groups one-way analysis of variance followed by Šidák post-hoc analysis. All data are presented as mean ± standard

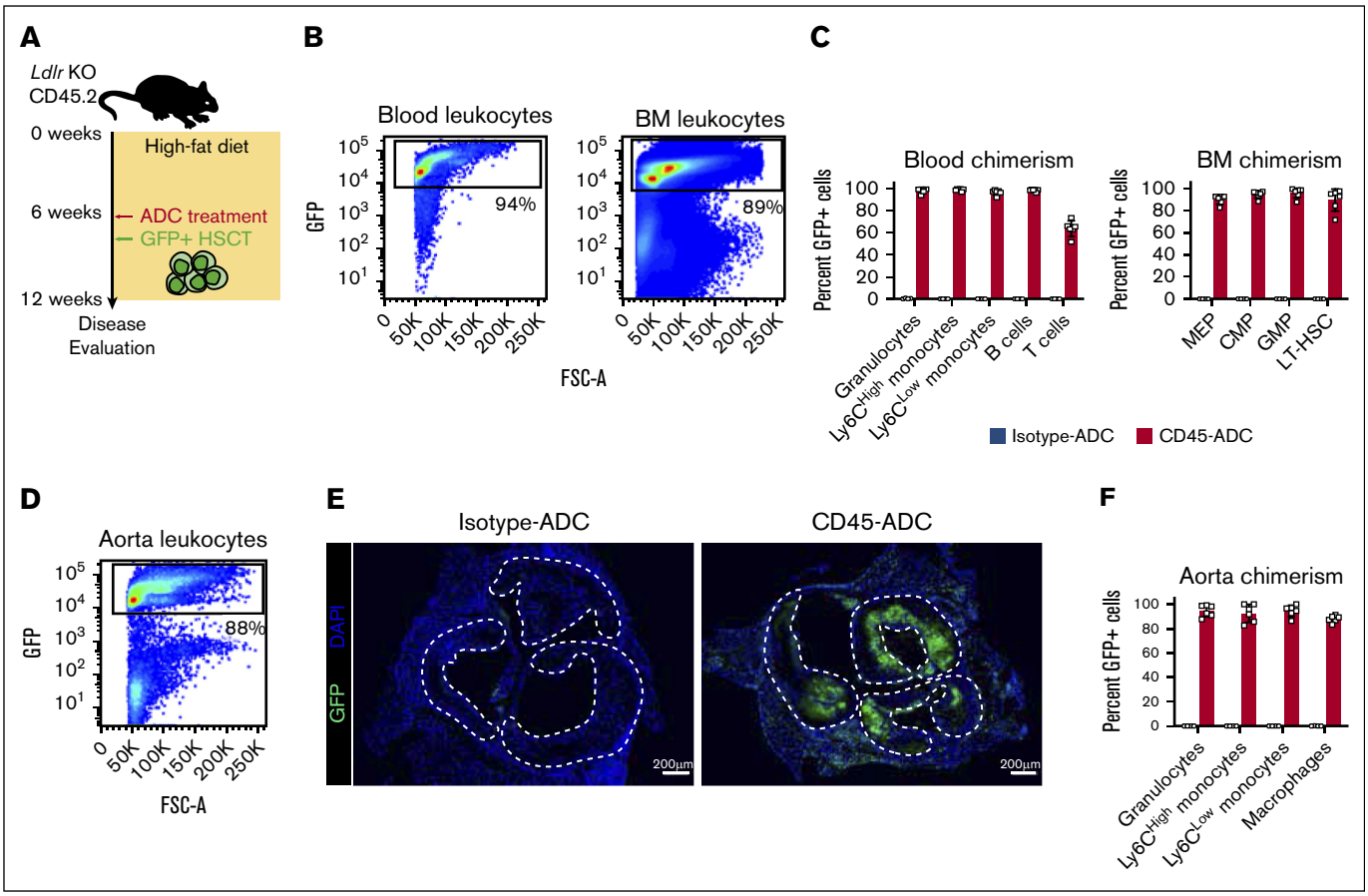

Figure 2. Effective myeloid cell replacement in atherosclerotic plaques after CD45-ADC conditioning. (A) Schematic illustration of the experimental design for atherosclerosis induction and CD45-ADC treatment and ubiquitin-GFP HSCT in Ldlr KO mice. (B) Representative flow plots showing the degree of GFP chimerism in the peripheral blood and bone marrow, 6 weeks after CD45-ADC treatment and HSCT in atherosclerotic Ldlr KO mice. (C) Bar graphs displaying the flow cytometric analysis of GFP chimerism in peripheral blood and bone marrow cell subsets, 6 weeks after CD45-ADC treatment and HSCT in atherosclerotic Ldlr KO mice. (D) FACS plot representative of hematopoietic GFP chimerism in aortic atherosclerotic lesions from Ldlr KO mice, 6 weeks after treatment with CD45-ADC and HSCT. (E) Immunofluorescence images of aortic roots from Ldlr KO mice stained for GFP (green) and DAPI (blue). Dashed lines outline atherosclerotic plaque surface area. Scale bar, 200 μm. (F) GFP chimerism in myeloid cell populations infiltrating aortic atherosclerotic plaques, 6 weeks after CD45-ADC treatment and HSCT of Ldlr KO mice, presented as bar graphs. CMP, common myeloid progenitor; GMP, granulocyte-monocyte progenitor; MEP, megakaryocyte-erythroid progenitor.

deviation, and statistical significance was set to $P < .05$, and significance is denoted as follows: $*P < .05$, $**P < .01$, $***P < .001$, and $****P < .0001$.

Results

CD45-ADC conditioning and tissue chimerism

We first assessed the efficiency of CD45-ADC treatment and HSCT in replacing tissue-resident myeloid cells in WT C57Bl/6 mice. The mice were treated with 3 mg/kg CD45-ADC or isotype-ADC followed by transplantation of 2.0×10^7 congenic bone marrow cells from *ubiquitin-GFP* donor mice (Figure 1A). As described previously, this resulted in depletion of endogenous cells and rapid engraftment of donor hematopoietic cells in blood and bone marrow, 6 weeks later in mice that received CD45-ADC treatment (Figure 1B-C; supplemental Figure 1A-B).[4] Recipients that were conditioned with isotype-ADC showed minimal GFP chimerism (Figure 1B-C; supplemental Figure 1A-B). Long-term hematopoietic stem cells (LT-HSCs) as well as myeloid progenitors (megakaryocytic-erythroid progenitors, common myeloid progenitors, and granulocyte-monocyte progenitors) all showed close to 90% engraftment (Figure 1C) and numbers of HSPCs had largely returned to baseline levels (supplemental Figure 1C). Relative to other immune cells, donor chimerism of peripheral blood T cells was lower (~60%, Figure 2C), likely because of the slow recovery of T-cell production after HSCT in combination with quiescent, peripheral T cells being less sensitive to the ADC payload.[4]

To determine how well various leukocyte types were depleted in nonhematopoietic tissues, we also collected brain, liver, lung, and skin tissue from the mice. Flow cytometric analysis of the hematopoietic fraction of these tissues revealed varying degrees of GFP chimerism. Although liver and lung displayed >70% GFP engraftment after CD45-ADC treatment, average skin GFP chimerism was 52% and, as expected, the brain showed little infiltration of graft-derived cells (Figure 1D; supplemental Figures 2A-D and 3A-D). This was further reflected in the

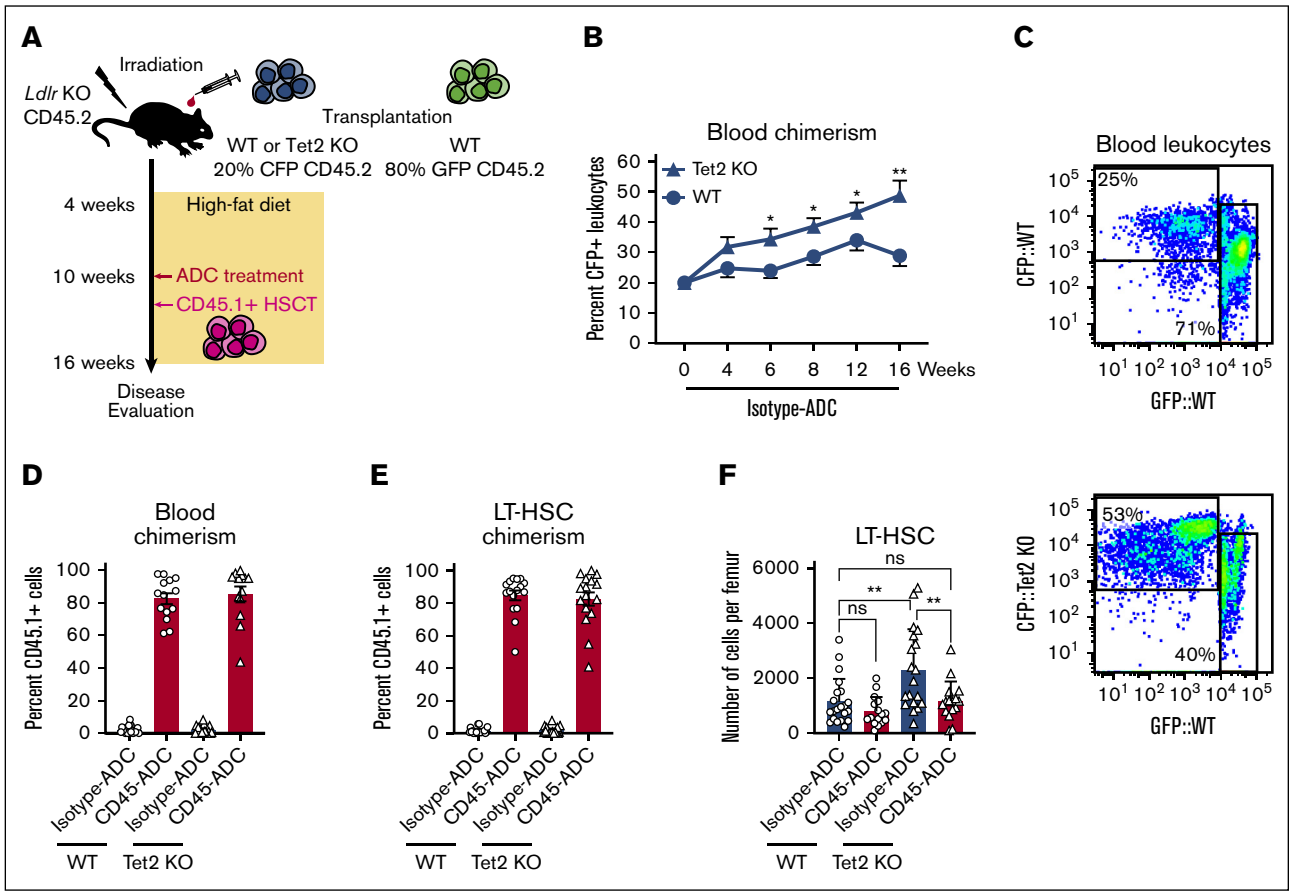

Figure 3. Depletion and replacement of *Tet2*-mutant HSPC after CD45-ADC conditioning. (A) Schematic depiction of the experimental outline for modeling Tet2 KO–driven clonal hematopoiesis and atherosclerosis. (B) Peripheral blood WT or Tet2 KO chimerism (CFP) in atherosclerotic Ldlr KO recipient mice, week 0 to 16 after bone marrow transplantation. (C) Representative FACS plots of CFP chimerism in the peripheral blood, 16 weeks after transplantation into Ldlr KO mice. (D) Bar graphs showing FACS analysis of CD45.1 chimerism, 6 weeks after CD45-ADC treatment, and CD45.1$^+$ HSCT in atherosclerotic Ldlr KO mice with either WT or Tet2 KO bone marrow. (E) FACS assessment of CD45.1 chimerism, 6 weeks after CD45-ADC treatment, and CD45.1$^+$ HSCT in atherosclerotic Ldlr KO mice with either WT or Tet2 KO bone marrow, displayed as bar graphs. (F) Number of LT-HSCs per femur in atherosclerotic Ldlr KO mice with either WT or Tet2 KO bone marrow, as determined by flow cytometric analysis.

analysis of individual myeloid cell types from these tissues. Immunophenotypic microglia that represent the largest population of hematopoietic cells in brain parenchyma (supplemental Figure 2A-B), showed little to no GFP labeling after CD45-ADC conditioning (Figure 1E). This is in line with the expectation of minimal uptake of antibodies across the blood–brain barrier.[25] Brain macrophages and monocytes, in contrast, are bone marrow derived and show significant GFP engraftment (Figure 1E). For the liver, lung, and skin, GFP engraftment was robust in most myeloid lineages after CD45-ADC conditioning, ranging from on average 60% to 90% (Figure 1E; supplemental Figures 2C-D and 3A-D); the 1 exception being the epidermal Langerhans cells that show an average GFP chimerism of 33% (Figure 1E). The epidermis of the skin is avascular, reducing antibody diffusion and, thus, most likely decreasing Langerhans cell depletion. Notably, bone marrow–derived, non–Kupffer cell macrophages are rarely found in the liver at steady state (supplemental Figure 2C-D), whereas we observed a substantial fraction of non–Kupffer cell macrophages 6 weeks after CD45-ADC and bone marrow infusion (supplemental Figure 2C-D). Tim4, the marker used for immunophenotypic identification of Kupffer cells, is, however, 1 of the last to be upregulated when bone marrow–derived cells differentiate into Kupffer cells.[26] Additionally, the combined number of immunophenotypic macrophages and Kupffer cells per liver was not different between CD45- and isotype-ADC–treated mice (supplemental Figure 2E), suggesting that the increased number of macrophages in the CD45-ADC cohort might merely be the result of the bone marrow–derived cells not having completed their maturation to Kupffer cells. In summary, this demonstrates that CD45-ADC conditioning and bone marrow hematopoietic cell infusion leads to efficient and rapid replacement of multiple TRM cell populations, many of which are bone marrow independent at homeostasis.

Near complete replacement of myeloid cells in atherosclerotic plaques after CD45-ADC conditioning and transplantation

Macrophages are drivers of atherosclerotic disease, and in advanced atherosclerotic plaques, local proliferation, rather than recruitment of bone marrow–derived monocytes, leads to their accumulation in atherosclerotic plaques.[13] We therefore tested whether HSCT after CD45-ADC conditioning would facilitate

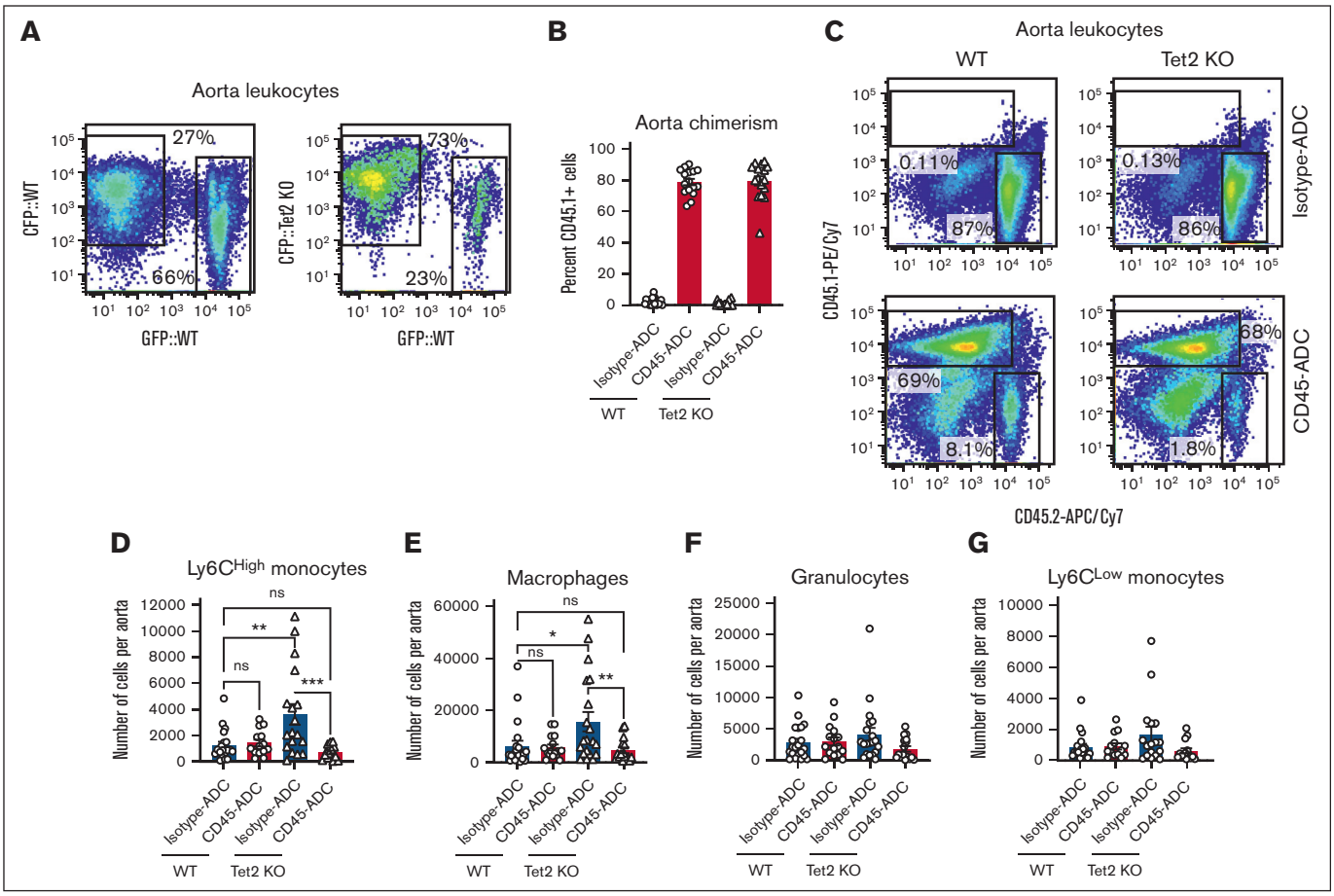

Figure 4. Clonal hematopoiesis driven atherosclerosis is mitigated by CD45-ADC and HSCT. (A) Representative flow plots showing the degree of CFP chimerism in atherosclerotic aortic lesions, 16 weeks after transplantation into Ldlr KO mice. (B) Bar graphs showing flow cytometric analysis of CD45.1 chimerism, 6 weeks after CD45-ADC treatment, and CD45.1$^+$ HSCT in atherosclerotic Ldlr KO mice with either WT or Tet2 KO bone marrow. (C) Flow plots representative of atherosclerotic aortic lesion CD45.1 chimerism after CD45-ADC treatment, and CD45.1$^+$ HSCT in Ldlr KO mice with either WT or Tet2 KO bone marrow. (D-G) Absolute numbers of various myeloid immune cells in aortic atherosclerotic plaques, 6 weeks after CD45-ADC treatment, and CD45.1$^+$ HSCT in Ldlr KO mice with either WT or Tet2 KO bone marrow, as analyzed by flow cytometry.

replacement of plaque macrophages in a murine model of atherosclerosis. As was done for WT recipient mice, *Ldlr* KO mice with established atherosclerotic lesions were conditioned with 3 mg/kg CD45-ADC or isotype-ADC and subsequently received transplantation with 2.0 × 10^7 congenic *ubiquitin-GFP* bone marrow cells (Figure 2A). Blood and bone marrow were isolated an additional 6 weeks after dosing, revealing similar high levels of GFP engraftment (Figure 2B); most bone marrow HSPCs and their respective mature lineages displayed >90% GFP chimerism in CD45-ADC–treated mice compared with isotype controls (Figure 2C; supplemental Figure 4A). The exception being that T lymphocytes, as was seen in WT recipients, had notably fewer GFP$^+$ cells (Figure 2C).

Analysis of aortic plaques from these mice demonstrated significant GFP engraftment in CD45-ADC-conditioned recipients (Figure 2D-E). Individual myeloid lineages, including plaque macrophages, also showed near complete replacement by GFP$^+$ cells in CD45-ADC–conditioned mice (Figure 2F; supplemental Figure 4B). Lastly, the absolute number of myeloid cell types was not different between CD45- and isotype-ADC–treated mice, suggesting that the tissue had returned to homeostasis after the transplantation (supplemental Figure 4C). Conditioning with CD45-ADC followed by bone marrow hematopoietic cell infusion thus enables efficient replacement of aortic plaque macrophages.

CD45-ADC conditioning and transplantation depletes *Tet2*-mutant HSPCs

Age-related clonal hematopoiesis is associated with atherosclerotic disease.[27,28] Clonal hematopoiesis arises when single LT-HSCs acquire certain mutations, which leads to bone marrow HSPCs producing increased numbers of myeloid progeny, and to mature myeloid cells secreting excess amounts of inflammatory cytokines in the case of Tet2 mutation.[29] To model clonal hematopoiesis, we set up bone marrow chimeras in atherosclerosis-prone *Ldlr* KO recipients, with these mice receiving transplantation with either 20% *Tet2* KO CFP$^+$ (*Tet2$^{fl/f}$MxCre-βactin-CFP)* and 80% WT GFP$^+$ (*ubiqutin-GFP*) bone marrow, or a 20% WT CFP$^+$ (*Tet2$^{WT/WT}$MxCre-βactin-CFP*) and 80% WT GFP$^+$ graft (Figure 3A). Highly efficient *Tet2* deletion was induced at 4 weeks (supplemental Figure 5A), and the mice were subsequently placed on a high-fat diet to initiate atherosclerosis. CD45- or isotype-ADC (3 mg/kg) treatment was given after 6 weeks of

disease development, and all mice received 2.0 × 10^7 congenic CD45.1$^+$ bone marrow cells (Figure 3A).

Tet2 KO gives mutant HSPCs a competitive advantage.[30] The proportion of *Tet2* mutant–derived cells in peripheral blood consequently increased with time when comparing isotype control–treated *Tet2* KO recipients with their WT counterparts (Figure 3B), and at 16 weeks after transplantation the average *Tet2* KO chimerism increased more than twofold (Figure 3B-C). This is also reflected in the bone marrow in which the vast majority of LT-HSCs were found to be *Tet2* KO at 16 weeks in the isotype-ADC cohort (supplemental Figure 5B). Despite this obvious competitive advantage, CD45-ADC and subsequent infusion of a WT bone marrow graft resulted in efficient replacement of *Tet2* KO cells in both the blood and LT-HSCs, as evident by the high degree of CD45.1 engraftment (Figure 3C-D). This also led to a normalization of white blood cell counts (supplemental Figure 5C) and numbers of LT-HSCs residing in the bone marrow when comparing *Tet2* KO recipients treated with CD45-ADC with controls (Figure 3E). Most aspects of *Tet2*-mutant clonal hematopoiesis in the blood and bone marrow were thus reversed by CD45-ADC conditioning and transplantation with WT bone marrow.

Clonal hematopoiesis–associated atherosclerosis is mitigated by CD45-ADC conditioning and WT hematopoietic cells

Tet2 KO leukocytes also displayed a selective advantage in atherosclerotic plaques isolated from the aorta of WT and *Tet2*-mutant recipients treated with isotype-ADC, 12 weeks after disease induction (Figure 4A; supplemental Figure 5D). Nonetheless, CD45-ADC and bone marrow hematopoietic cell infusion lead to efficient replacement of *Tet2* KO cells in atherosclerotic lesions, 6 weeks after conditioning, as evidenced by the high degree of CD45.1$^+$ chimerism (Figure 4B-C). This also resulted in the normalization of multiple parameters in CD45-ADC–treated *Tet2* KO recipients. Overall aorta cellularity was reduced to WT quantities (supplemental Figure 5E) and numbers of Ly6C^{High} monocytes as well as macrophages also returned to levels similar to what was observed in WT controls (Figure 4D-E). Aortic granulocyte and Ly6C^{Low} monocytes remained unchanged across genotype and treatments (Figure 4F-G). Next, we assessed aortic plaque size as a measure of disease burden. As has been described by others, we observed that *Tet2*-mutant leukocytes contributed to increased atherosclerotic plaques in aortic roots compared with WT controls (Figure 5). Plaque burden was however specifically reduced in *Tet2* KO recipients treated with CD45-ADC and WT bone marrow cells (Figure 5), suggesting that clonal hematopoiesis–driven atherosclerosis can be reversed if mutant HSPCs and mature myeloid leukocytes are replaced by WT cells.

Discussion

TRM cells are key participants in tissue homeostasis and, as such, may also be drivers of disease. A wide range of diseases can thus be cured if TRM cells could be replaced efficiently. We report that a single dose of reduced-toxicity ADC conditioning and adoptive hematopoietic cells can replace TRM cells and enable a therapeutic effect.

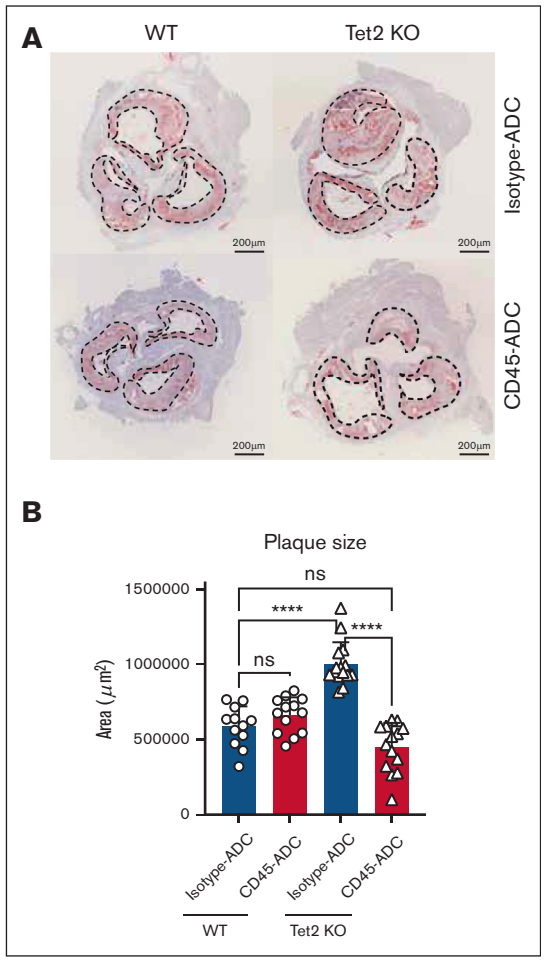

Figure 5. CD45-ADC and HSCT reduces aortic root plaque burden in clonal hematopoiesis driven atherosclerosis. (A) Oil-red-O images of aortic roots, 6 weeks after CD45-ADC treatment, and CD45.1$^+$ HSCT in Ldlr KO mice with either WT or Tet2 KO bone marrow. Dashed lines outline atherosclerotic plaque surface area. Scale bar, 200 μm. (B) Quantification of aortic root atherosclerotic lesion surface area, 6 weeks after CD45-ADC treatment, and CD45.1$^+$ HSCT in Ldlr KO mice with either WT or Tet2 KO bone marrow.

HSCT is a curative alternative for metabolic storage diseases like Hurler syndrome or Gaucher disease, because it is well established that radiation or chemotherapy conditioning ablates native TRM cells, allowing for replacement of the disease-causing cells upon transplantation.[31,32] However, because of the morbidity and mortality associated with standard conditioning regimens, many patients do not receive this treatment. Instead, they may rely on lifelong, costly, and time-consuming enzyme replacement therapies, if they are available. Yet, previous experimental work suggests that only 10% of the mutant macrophages need to be replaced to achieve disease modification.[33] CD45-ADC conditioning followed by bone marrow infusion led to a minimum of 30% TRM cell engraftment efficiency but for most peripheral tissues TRM cell replacement was between 80% and 90%. One major limitation is the absence of microglial replacement, although approximately half of central nervous system monocytes and macrophages were from the graft. Whether those cells would be sufficient to enable a therapeutic effect is unknown.

Previous work in mouse models using radiation conditioning has shown that host-derived TRM cells will repopulate tissues if the incoming HSCT graft has an inherent deficiency in macrophage maintenance.[10] It was therefore unclear whether WT-derived myeloid cells would be able to outcompete *Tet2*-mutant macrophages in atherosclerotic lesions, given their competitive disadvantage.[29] *Tet2* KO macrophage replacement was however nearly complete and resulted in a significant reduction in atherosclerotic plaque burden, suggesting that CD45-ADC treatment is highly efficient at ablating TRM cells. There are currently no treatments that target clonal hematopoiesis, but these results suggest that some form of TRM cell–replacement strategy might be helpful.

For both metabolic storage disease and clonal hematopoiesis–exacerbated atherosclerosis, complete replacement of the hematopoietic system would be an extreme measure but it may not be needed. It is reported that most TRM cells become self-sustaining once established in their respective tissues.[13,15] Follow-up studies will determine whether durable TRM cell chimerism can be achieved with lower doses of ADC and only mature or progenitor level myeloid cell infusions. If so, it is possible to envision using ADC to ablate mutant host-derived cells and follow-up with infusion of gene-corrected myeloid progenitors or mature macrophages. Indeed, in animal models of hereditary pulmonary alveolar proteinosis, disease-causing *CSF2RA/B* mutant macrophages can be durably replaced by WT macrophages, leading to disease correction.[34] Our data suggest that the CD45-ADC may enable such an approach for additional conditions.

Remarkably, in all tested tissues in which TRM cell replacement occurred after CD45-ADC conditioning, cell numbers returned to baseline levels (supplemental Figures 2B,D-E, 3B,D, and 4C). A similar phenomenon was observed in the aortic plaques. When macrophage numbers were normalized to plaque size, there was no difference across genotypes or treatment groups (supplemental Figure 5F). The latter observation is in line with what others have reported in the context of *Tet2*-mutant atherosclerosis.[29] This supports the idea that the surrounding tissue regulates the size of its TRM population,[35] perhaps by TRM "niches" regulating TRM cell persistence in a highly restricted manner.

In summary, this study provides proof-of-concept that targeted, reduced-toxicity CD45-ADC conditioning and hematopoietic cell adoptive transfer can be used to replace TRM cells, achieving a therapeutic effect in clonal hematopoiesis–driven atherosclerotic disease. Furthermore, in other diseases in which TRM cells participate, a similar strategy can be envisioned by using TRM cell replacement with either WT or perhaps hematopoietic cells expressing therapeutic proteins in other disease settings in which TRM cells participate.

Acknowledgments

The authors thank members of D.T.S. and M.N. laboratories for technical assistance. The authors acknowledge support with expert technical assistance from the Harvard Stem Cell Institute-Center for Regeneative Medicine Flow Cytometry facility.

This research was supported by the Craig A. Huff Harvard Stem Cell Institute Research Support Fund, the Gerald and Darlene Jordan Professorship of Medicine, and the National Institutes of Health U19AI149676 (D.T.S.) K.G. was supported by the Swedish Research Council and the John S. Macdougall Jr and Olive R. Macdougall Fund.

Authorship

Contribution: K.G., M.N., and D.T.S. conceived the study; K.G. and V.F. designed and performed most of the experiments with technical assistance from and discussions with C.R., D.L., and E.W.S.; Y.I. performed all tissue processing for histological analysis; R.P., S.L.H., and A.E.B. discussed data, and edited the manuscript; K.G. and D.T.S. interpreted the data, and wrote the manuscript; and all authors read, edited, and approved the manuscript.

Conflict-of-interest disclosure: D.T.S. is a director and shareholder for Agios Therapeutics and Editas Medicines; is a founder and director of, shareholder in, and scientific advisory board member for, Magenta Therapeutics and LifeVault Bio; is a shareholder in, and founder of, Fate Therapeutics and Garuda Therapeutics; is a director and founder of, and shareholder in Clear Creek Bio; is a consultant for FOG Pharma, Inzen Therapeutics, and Vcanbio; and is a recipient of sponsored research funding from Sumitomo Dainippon. D.T.S. and K.G. are inventors of patent US20220143099A1. R.P., S.L.H., and A.E.B. were full-time salaried employees and equity holders of Magenta Therapeutics at the time the work was completed.

ORCID profiles: V.F., 0000-0001-5566-6692; M.N., 0000-0002-4021-1887; D.T.S., 0000-0001-9821-7133.

Correspondence: David T. Scadden, Center for Regenerative Medicine, Harvard Stem Cell Institute, Massachusetts General Hospital, 185 Cambridge St, Boston, MA 02114; email: david_scadden@harvard.edu.

References

1. Chandrakasan S, Jayavaradhan R, Ernst J, et al. KIT blockade is sufficient for donor hematopoietic stem cell engraftment in Fanconi anemia mice. *Blood*. 2017;129(8):1048-1052.
2. Czechowicz A, Palchaudhuri R, Scheck A, et al. Selective hematopoietic stem cell ablation using CD117-antibody-drug-conjugates enables safe and effective transplantation with immunity preservation. *Nat Commun*. 2019;10(1):617.
3. Palchaudhuri R, Saez B, Hoggatt J, et al. Non-genotoxic conditioning for hematopoietic stem cell transplantation using a hematopoietic-cell-specific internalizing immunotoxin. *Nat Biotechnol*. 2016;34(7):738-745.
4. Saha A, Hyzy S, Lamothe T, et al. A CD45-targeted antibody-drug conjugate successfully conditions for allogeneic hematopoietic stem cell transplantation in mice. *Blood*. 2022;139(11):1743-1759.

5. Fu Z, Li S, Han S, Shi C, Zhang Y. Antibody drug conjugate: the "biological missile" for targeted cancer therapy. *Signal Transduct Target Ther*. 2022;7(1):93.
6. Ginhoux F, Greter M, Leboeuf M, et al. Fate mapping analysis reveals that adult microglia derive from primitive macrophages. *Science*. 2010;330(6005):841-845.
7. Hoeffel G, Ginhoux F. Fetal monocytes and the origins of tissue-resident macrophages. *Cell Immunol*. 2018;330:5-15.
8. Gomez Perdiguero E, Klapproth K, Schulz C, et al. Tissue-resident macrophages originate from yolk-sac-derived erythro-myeloid progenitors. *Nature*. 2015;518(7540):547-551.
9. Hoeffel G, Chen J, Lavin Y, et al. C-Myb(+) erythro-myeloid progenitor-derived fetal monocytes give rise to adult tissue-resident macrophages. *Immunity*. 2015;42(4):665-678.
10. Hashimoto D, Chow A, Noizat C, et al. Tissue-resident macrophages self-maintain locally throughout adult life with minimal contribution from circulating monocytes. *Immunity*. 2013;38(4):792-804.
11. Bleriot C, Dupuis T, Jouvion G, Eberl G, Disson O, Lecuit M. Liver-resident macrophage necroptosis orchestrates type 1 microbicidal inflammation and type-2-mediated tissue repair during bacterial infection. *Immunity*. 2015;42(1):145-158.
12. Remmerie A, Martens L, Thone T, et al. Osteopontin expression identifies a subset of recruited macrophages distinct from Kupffer cells in the fatty liver. *Immunity*. 2020;53(3):641-657.e14.
13. Robbins CS, Hilgendorf I, Weber GF, et al. Local proliferation dominates lesional macrophage accumulation in atherosclerosis. *Nat Med*. 2013;19(9):1166-1172.
14. Haniffa M, Ginhoux F, Wang XN, et al. Differential rates of replacement of human dermal dendritic cells and macrophages during hematopoietic stem cell transplantation. *J Exp Med*. 2009;206(2):371-385.
15. Lavin Y, Winter D, Blecher-Gonen R, et al. Tissue-resident macrophage enhancer landscapes are shaped by the local microenvironment. *Cell*. 2014;159(6):1312-1326.
16. Perdiguero EG, Geissmann F. The development and maintenance of resident macrophages. *Nat Immunol*. 2016;17(1):2-8.
17. Guilliams M, Thierry GR, Bonnardel J, Bajenoff M. Establishment and maintenance of the macrophage niche. *Immunity*. 2020;52(3):434-451.
18. Jenkins SJ, Allen JE. The expanding world of tissue-resident macrophages. *Eur J Immunol*. 2021;51(8):1882-1896.
19. Malosse C, Henri S. Isolation of mouse dendritic cell subsets and macrophages from the skin. *Methods Mol Biol*. 2016;1423:129-137.
20. Guldner IH, Golomb SM, Wang Q, Wang E, Zhang S. Isolation of mouse brain-infiltrating leukocytes for single cell profiling of epitopes and transcriptomes. *STAR Protoc*. 2021;2(2):100537.
21. Andreata F, Bleriot C, Di Lucia P, et al. Isolation of mouse Kupffer cells for phenotypic and functional studies. *STAR Protoc*. 2021;2(4):100831.
22. Daemen S, Chan MM, Schilling JD. Comprehensive analysis of liver macrophage composition by flow cytometry and immunofluorescence in murine NASH. *STAR Protoc*. 2021;2(2):100511.
23. Atif SM, Gibbings SL, Jakubzick CV. Isolation and identification of interstitial macrophages from the lungs using different digestion enzymes and staining strategies. *Methods Mol Biol*. 2018;1784:69-76.
24. Christofides A, Cao C, Pal R, Aksoylar HI, Boussiotis VA. Flow cytometric analysis for identification of the innate and adaptive immune cells of murine lung. *J Vis Exp*. 2021;(177).
25. Terstappen GC, Meyer AH, Bell RD, Zhang W. Strategies for delivering therapeutics across the blood-brain barrier. *Nat Rev Drug Discov*. 2021;20(5):362-383.
26. Guilliams M, Scott CL. Liver macrophages in health and disease. *Immunity*. 2022;55(9):1515-1529.
27. Jaiswal S, Fontanillas P, Flannick J, et al. Age-related clonal hematopoiesis associated with adverse outcomes. *N Engl J Med*. 2014;371(26):2488-2498.
28. Jaiswal S, Natarajan P, Silver AJ, et al. Clonal hematopoiesis and risk of atherosclerotic cardiovascular disease. *N Engl J Med*. 2017;377(2):111-121.
29. Fuster JJ, MacLauchlan S, Zuriaga MA, et al. Clonal hematopoiesis associated with TET2 deficiency accelerates atherosclerosis development in mice. *Science*. 2017;355(6327):842-847.
30. Moran-Crusio K, Reavie L, Shih A, et al. Tet2 loss leads to increased hematopoietic stem cell self-renewal and myeloid transformation. *Cancer Cell*. 2011;20(1):11-24.
31. Aldenhoven M, Wynn RF, Orchard PJ, et al. Long-term outcome of Hurler syndrome patients after hematopoietic cell transplantation: an international multicenter study. *Blood*. 2015;125(13):2164-2172.
32. Erikson A, Groth CG, Mansson JE, Percy A, Ringden O, Svennerholm L. Clinical and biochemical outcome of marrow transplantation for Gaucher disease of the Norrbottnian type. *Acta Paediatr Scand*. 1990;79(6-7):680-685.
33. Enquist IB, Nilsson E, Mansson JE, Ehinger M, Richter J, Karlsson S. Successful low-risk hematopoietic cell therapy in a mouse model of type 1 Gaucher disease. *Stem Cells*. 2009;27(3):744-752.
34. Suzuki T, Arumugam P, Sakagami T, et al. Pulmonary macrophage transplantation therapy. *Nature*. 2014;514(7523):450-454.
35. Zhou X, Franklin RA, Adler M, et al. Microenvironmental sensing by fibroblasts controls macrophage population size. *Proc Natl Acad Sci U S A*. 2022;119(32):e2205360119.